2026 IEEE Intelligent Vehicles Symposium (IV)
June 22-25, 2026. Detroit, MI, USA

Learning human driver dynamics from experiments

Bence Szaksz, Xunbi A. Ji, Tamas G. Molnar, Sergei S. Avedisov, Gábor Stepan, and Gábor Orosz

2026 IEEE Intelligent Vehicles Symposium (IV) | 979-8-3315-4793-6/26/$31.00 ©2026 IEEE | DOI: 10.1109/IV66570.2026.11623895

Abstract*—Human driving dynamics are learned from real field experiments using artificial intelligence (AI), more precisely, using time delay neural networks (TDNNs), which provide a compact way to capture real traffic behavior, up to bistability. The experiments are conducted utilizing the virtual ring concept where an automated vehicle (AV) is driving in front of several human-driven vehicles (HVs), while receiving the position and velocity of the last HV of the chain via wireless vehicle-to-everything (V2X) communication. The AV uses this information in its controller to close the virtual ring. It is shown that for certain control parameters, this system exhibits bistable behavior, where it either approaches a steady state or sustained oscillations develop, depending on perturbations. The human driving dynamics is learned by using TDNNs, which capture the nonlinear equation of motion as well as the reaction time delay. We demonstrate that once these networks are substituted into the virtual ring model, bistable behavior develops, confirming the predictive capabilities of the corresponding neural delay differential equation (NDDE). The results support a better understanding of human driving dynamics, which helps in adjusting the control of self-driving vehicles to handle mixed traffic situations.

I. INTRODUCTION

Highly automated vehicles are becoming increasingly common in multiple major cities around the world. Furthermore, an increasing number of production vehicles are equipped with partial automation like adaptive cruise control [1]–[5]. Still, for a long time, human-driven vehicles (HVs) will continue to dominate traffic. During this transitional period, automated vehicles (AVs) must be prepared to operate safely and efficiently in mixed traffic environments that include both AVs and HVs [6]. Designing control strategies for such mixed traffic requires a thorough understanding of human driving behavior. Data-driven model identification for this purpose demands a relatively large amount of high-quality data that include various traffic scenarios ranging from free flow highway traffic to congestion and even accidents.

Bence Szaksz is with the Department of Applied Mechanics, and with the MTA-BME Lendulet "Momentum" Global Dynamics Research Group, Budapest University of Technology and Economics, Budapest, H-1111, Hungary. szaksz@mm.bme.hu.

Xunbi Ji, Sergei Avedisov, and Gábor Orosz are with the Department of Mechanical Engineering, University of Michigan, Ann Arbor, MI 48109, USA. {xunbij, avediska, orosz}@umich.edu.

Tamas G. Molnar is with the Department of Mechanical Engineering, Wichita State University, Wichita, KS 67260, USA. tamas.molnar@wichita.edu.

Gábor Stepan is with the Department of Applied Mechanics, and with the HUN-REN–BME Dynamics of Machines Research Group, Budapest University of Technology and Economics, Budapest, H-1111, Hungary. stepan@mm.bme.hu.

Bence Szaksz is also with the Department of Mechanical Engineering, University of Michigan, Ann Arbor, MI 48109, USA.

Gábor Orosz is also with the Department of Civil and Environmental Engineering, University of Michigan, Ann Arbor, MI 48109, USA.

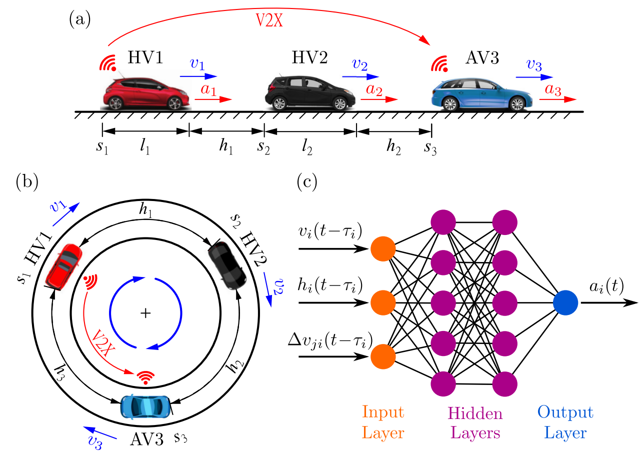

Fig. 1. (a) Virtual Ring setup: The automated vehicle AV3 drives in front of two human driven vehicles, while it receives the position and velocity of the last HV via V2X communication. The control of AV3 is designed in a way as if HV1 was in front of it. (b) The corresponding ring configuration. (c) Time delay neural network with two hidden layers, which was applied to learn the human driving dynamics.

One of the key measures in car-following dynamics is string stability, which describes whether oscillations initiated by a leading vehicle amplify or decay as they propagate along a chain of vehicles [7], [8]. Although string instability in human-driven vehicle chains is often observed on highways, conducting large-scale experiments to study this phenomenon is challenging. One way to solve this issue is to place the vehicles on a closed ring, which enables the observation of complex dynamical behavior with a small number of vehicles [9]–[11]. However, this ring configuration introduces a limitation: drivers must continuously compensate for lateral acceleration. For example, traveling at a realistic highway speed of 25 m/s on a ring of 70 m radius results in a centrifugal acceleration of about 1 g. Achieving realistic velocities with negligible lateral accelerations would therefore require impractically large rings.

To address this issue, the concept of virtual rings has been introduced [6], [12], [13]. In this setup, an automated vehicle drives ahead of several HVs while receiving the position and velocity of the last vehicle via vehicle-to-everything (V2X) communication, see Fig. 1. The AV's control is designed as if the last HV was projected in front of it. Consequently, when the AV brakes, the deceleration wave propagates through the vehicle chain until the last HV also brakes. At that point, the AV will brake in response to the virtual projection of the HV. This closes the virtual ring. This approach allows vehicles to drive on a straight road at realistic speeds while still exhibiting nonlinear human driving effects within a relatively small number of cars.

Data-based learning of dynamical behavior has rich literature, with numerous applicable methods including Bayesian approaches [14], [15], spectral submanifolds [16], [17], Sparse Identification of Nonlinear Dynamics (SINDy) [18], [19], extended dynamic mode decomposition (EDMD) [20] and neural networks [21], [22]. An additional challenge in modeling human driving dynamics is accounting for the non-negligible human reaction time, which introduces delay into the system. From a mathematical perspective, delayed dynamical systems have infinite-dimensional state spaces [23]; still, there are already existing approaches to learn the corresponding intricate dynamical behavior [24]–[26].

This study employs a model-free time delay neural network (TDNN) to learn human driving behavior from real-world traffic data, an area with a limited number of studies in the literature. As individual driving styles vary, and even the same driver may respond differently to identical situations depending on their level of concentration, learning human driving dynamics is inherently challenging. In this paper, we aim to describe human driving behavior using the simplest nontrivial model that accounts for the vehicle's own velocity, the headway, and the relative velocity with respect to the vehicle ahead, all considered with relevant time delays, see Fig. 1. We demonstrate that this approach can adequately capture human driving behavior. In particular, using the TDNNs in the virtual ring setup, the arising neural delay differential equation (NDDE) can reproduce bistable behavior observed in the experiments: small perturbations decay and the system returns to steady state while sufficiently large perturbations lead to sustained oscillations. The learned human driving dynamics provide essential insights for the AV control design, contributing to improved traffic efficiency and safety in mixed traffic scenarios.

The paper is organized as follows. The details of the virtual ring experiment are explained in Sec. II. Section III presents the structure of the TDNN applied to learn human driving dynamics. Then, the corresponding results are discussed in Sec. IV, including the demonstration of the bistable dynamics under certain parameter combinations. Finally, we add some concluding remarks in Sec. V.

II. EXPERIMENTS

Real field experiments were carried out with two HVs and one AV, each of them equipped with a V2X kit which includes an antenna for communication and an on-board unit (OBU) that was connected to a laptop via an Ethernet cable. This way, the vehicles could share their GPS-based position and velocity using the updated rate of 10 Hz. Since we were primarily interested in the longitudinal dynamics, the experiments were conducted on a straight road with low traffic. Fig. 1(a) illustrates the virtual ring setup: the AV travels in front, followed by two HVs. The numbering of the vehicles and their corresponding velocities and headways are assigned from back to front; that is, the last and middle HVs are labeled as #1 and #2, respectively, while the AV is denoted as #3. The position and velocity of HV1 are sent to the AV. The control of the AV is designed assuming that HV1 is located ahead of it, leading to the ring configuration in Fig. 1(b).

Let L denote the net ring length, that is, the sum of the headways, which does not include the lengths of the vehicles. Then, the equation of motion of the three vehicles on the virtual ring assumes the form

$$\dot{h}_1(t) = v_2(t) - v_1(t)\,, \tag{1}$$
$$\dot{h}_2(t) = v_3(t) - v_2(t)\,, \tag{2}$$
$$\dot{v}_1(t) = f_{\mathrm{HV1}}(h_1(t-\tau_1), v_1(t-\tau_1), \Delta v_{21}(t-\tau_1))\,, \tag{3}$$
$$\dot{v}_2(t) = f_{\mathrm{HV2}}(h_2(t-\tau_2), v_2(t-\tau_2), \Delta v_{32}(t-\tau_2))\,, \tag{4}$$
$$\dot{v}_3(t) = f_{\mathrm{AV3}}(h_3(t-\sigma), v_3(t-\sigma), \Delta v_{13}(t-\sigma))\,, \tag{5}$$

where τ_1, τ_2 and σ are the time delays of HV1, HV2 and AV3, respectively, while Δv_{ij} refers to the relative velocity

$$\Delta v_{ij} = v_i - v_j\,. \tag{6}$$

Finally, fixing L provides a geometric constraint for the virtual headway of the AV:

$$h_3 = L - (h_1 + h_2)\,. \tag{7}$$

In the above equations of motion, we assumed that each human driver controls the longitudinal dynamics of the vehicle based on its headway, velocity and relative velocity with respect to the preceding vehicle. Moreover, all these inputs are considered to be subject to the same constant time delay τ_i $(i = 1, 2)$ that contains both the reaction time of the driver and the response time of the vehicle. Note that there may be other influencing factors, for example, the blinking brake light of the preceding vehicle or the variation of the human reaction time depending on the concentration level. Still, our model is reasonable: it is the simplest nontrivial one that describes the essential human driver dynamics. In the following section, the developed TDNN is trained to capture such a driver model, see also Fig. 1(c).

The control of the AV is based on the optimal velocity model [5], [27], [28]. It consists of two parts: the control of the headway with gain α, and the control of the velocity difference with respect to the preceding vehicle using the gain β, yielding the commanded acceleration

$$u_3 = \alpha\big(V(h_3) - v_3\big) + \beta\big(W(v_1) - v_3\big)\,. \tag{8}$$

The term $W(v)$ denotes the speed policy

$$W(v) = \min(v, v_{\max})\,, \tag{9}$$

with $v_{\max}$ as the maximum allowed speed on the road. Finally, $V(h)$ stands for the piecewise linear range policy

$$V(h) = \begin{cases} 0, & \text{if } h < h_{\mathrm{st}}\,, \\ v_{\max}\frac{h-h_{\mathrm{st}}}{h_{\mathrm{go}}-h_{\mathrm{st}}}, & \text{if } h_{\mathrm{st}} \le h \le h_{\mathrm{go}}\,, \\ v_{\max}, & \text{if } h > h_{\mathrm{go}}\,. \end{cases} \tag{10}$$

Accordingly, if the headway is larger than a prescribed value h_{go}, then the vehicle can cruise with $v_{\max}$, while if the headway is too small, that is, $h < h_{\mathrm{st}}$, then the vehicle aims to stop. For moderately large headway $h_{\mathrm{st}} \le h \le h_{\mathrm{go}}$, the

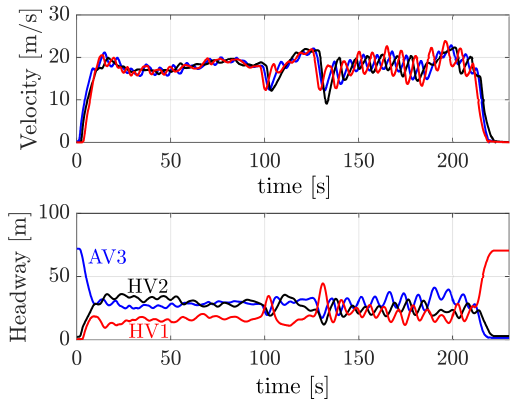

Fig. 2. Representative time series from the experiment for $L = 75\,\mathrm{m}$, $h_{\mathrm{go}} = 42.5\,\mathrm{m}$. The red, black and blue colors refer to the vehicles HV1, HV2 and AV3, respectively. Initially the equilibrium seems to be stable, then at $t \approx 100\,\mathrm{s}$ and at $t \approx 130\,\mathrm{s}$ HV1 brakes intentionally. These cause oscillations in the speeds, which decay in the first case, but then persist in the second case, indicating bistability.

appropriate velocity is adjusted to the actual value of the headway; for simplicity, this relationship is governed by a linear function.

In reality, both the acceleration and the deceleration of the vehicles are limited, thus, the final equation of motion of the AV takes the form

$$\dot{v}_3(t) = \mathrm{sat}(u_3(t-\sigma))\,, \tag{11}$$

where the saturation function of the control assumes the form

$$\mathrm{sat}(u) = \begin{cases} u_{\min}, & \text{if } u < u_{\min}\,, \\ u, & \text{if } u_{\min} \le u \le u_{\max}\,, \\ u_{\max}, & \text{if } u > u_{\max}\,. \end{cases} \tag{12}$$

The control parameters of the AV used in the experiments are summarized in Table I, including the measured time delay σ.

Figure 2 depicts an example measurement. The vehicles started from standstill, they accelerated to $20\,\mathrm{m/s}$ in approximately 15 seconds, and then they kept that speed for a while to see whether the virtually closed vehicle chain is stable for small perturbations. As it was the case, the human driver of vehicle $\#1$ intentionally steps on the brake, imposing a large perturbation to the system. This deceleration causes the virtual headway in front of AV3 to decrease, forcing it to brake, and the braking wave travels backward along the virtual ring. Depending on the size of the perturbation, this oscillation either dies out (the system returns to the previous steady state motion), or leads to long-lasting self-excited oscillations. In extreme cases, after a certain time, AV3 stops, and so the other two vehicles stop behind it as well, then AV3 starts moving again, and so on.

We investigated three different control setups of the AV, in particular, the free-flow headway h_{go} was selected as $35\,\mathrm{m}$, $42.5\,\mathrm{m}$, and $55\,\mathrm{m}$, which yield a relatively aggressive, a moderate and a gentle driving style, respectively. Furthermore, the net ring length L was also varied between $15\,\mathrm{m}$ and $120\,\mathrm{m}$.

TABLE I
PARAMETERS OF AUTOMATED VEHICLE.

h_{st} [m]	h_{go} [m]	$v_{\max}$ [m/s]	α [1/s]	β [1/s]	σ [s]	$u_{\min}$ [m/s^2]	$u_{\max}$ [m/s^2]
5	$35, 42.5, 55$	30	0.4	0.5	0.6	-7	3

III. LEARNING HUMAN DRIVER DYNAMICS

In this section, we identify the human driving behavior from the experimental data using a time delay neural network (TDNN).

The TDNN is structured as follows, see also Fig. 1(c). The input vector $\mathbf{x}$ consists of the delayed functions of the velocity, headway and relative velocity:

$$\mathbf{x} = \begin{bmatrix} v(t-\tau) \\ h(t-\tau) \\ \Delta v(t-\tau) \end{bmatrix}, \tag{13}$$

while the scalar output is the actual acceleration $a(t) = \dot{v}(t)$. In between, there are two hidden layers with 5-5 neurons. In order to obtain a differentiable network, the elementwise $\tanh_{\mathrm{e}}$ functions are selected as activation functions, so the mathematical representation takes the form:

$$\mathrm{net}(\mathbf{x}) = \mathbf{W}_3 \tanh_{\mathrm{e}}(\mathbf{W}_2 \tanh_{\mathrm{e}}(\mathbf{W}_1 \mathbf{x} + \mathbf{b}_1) + \mathbf{b}_2)\,, \tag{14}$$

where $\mathbf{W}_1 \in \mathbb{R}^{5\times3}$, $\mathbf{W}_2 \in \mathbb{R}^{5\times5}$, and $\mathbf{W}_3 \in \mathbb{R}^{1\times5}$ denote the weight matrices, while $\mathbf{b}_1 \in \mathbb{R}^{5\times1}$ and $\mathbf{b}_2 \in \mathbb{R}^{5\times1}$ are the bias vectors.

During data preparation, the useful time windows corresponding to car following are cut out from the raw data. When the dynamics of HV2 is learned, this means that only the unnecessary parts at the beginning and at the end of each run are removed. However, as it was discussed earlier, the driver of HV1 sometimes performed intentional braking to perturb the system, during which that vehicle does not respond to the car in the front. Thus, when the dynamics of HV1 is learned, these periods of intentional braking must also be removed.

We use Glorot initialization for the weights $\mathbf{W}_1$, $\mathbf{W}_2$, and $\mathbf{W}_3$ [29], the biases $\mathbf{b}_1$ and $\mathbf{b}_2$ are initialized as zero vectors, while the initial guess for the time delay is selected as $0.4\,\mathrm{s}$.

When learning the dynamics of vehicle i, the algorithm selects 200 random time instances t_k $(k = 1, \ldots, 200)$ from each measurement, then the code extracts the velocity $v_i(t_k - \tilde{\tau}_i)$, headway $h_i(t_k - \tilde{\tau}_i)$, and relative velocity $\Delta v_{i+1,i}(t_k - \tilde{\tau}_i)$, where $\tilde{\tau}_i$ is the currently estimated time delay. Note that in general the delay is not an integer multiple of the sampling time step, thus, the delayed states are obtained via interpolation. Then, using the actual weights and biases, the TDNN calculates the estimated acceleration $\tilde{a}_i(t_k)$. In the loss function, this is compared to the real acceleration $a_i(t_k)$ obtained from the measurements:

$$L = \frac{1}{N} \sum_{k=1}^{N} (\tilde{a}_i(t_k) - a_i(t_k))^2\,, \tag{15}$$

where N is the total number of time instances in the current epoch. This loss function depends on the trainable parameters $\theta_{\mathrm{p}} = \{\mathbf{W}_1, \mathbf{W}_2, \mathbf{W}_3, \mathbf{b}_1, \mathbf{b}_2\}$ and on the trainable delay $\theta_\tau = \{\tau_i\}$.

The algorithm then calculates the gradients

$$g_{\mathrm{p}} = \frac{\partial L}{\partial \theta_{\mathrm{p}}}\,, \quad g_\tau = \frac{\partial L}{\partial \theta_\tau}\,, \tag{16}$$

which are used to obtain the updated parameters via adaptive moment estimation [30]. It is based on two stochastic gradient descent approaches: the adaptive gradients and the root mean square propagation. The corresponding update takes the form:

$$\theta_{n+1} = \theta_n - \frac{\eta}{\sqrt{\hat{r}_n} + \epsilon}\hat{m}_n\,, \tag{17}$$

where η is the learning rate, ϵ is a small constant preventing division by zero, while

$$\hat{m}_n = \frac{m_n}{1-\beta_1^n}\,, \quad \hat{r}_n = \frac{r_n}{1-\beta_2^n}\,. \tag{18}$$

Here m_n and r_n are estimates for the first moment and second moment, respectively. They are updated according to the rule

$$m_n = \beta_1 m_{n-1} + (1-\beta_1) g_n\,, \tag{19}$$

$$r_n = \beta_2 r_{n-1} + (1-\beta_2) g_n^2\,, \tag{20}$$

where g_n is the gradient in the n-th step, while β_1 and β_2 are the gradient decay factor and the squared gradient decay factor, respectively.

IV. Results

When learning the human driver dynamics, the maximum epoch number was set to 2000. We used $\eta_\tau = 0.005$ as the learning rate of the delay, $\eta_{\mathrm{p}} = 0.01$ as the learning rate of the other parameters, while ϵ, β_1 and β_2 were set to 10^{-8}, 0.9, 0.999, respectively.

The driving dynamics was learned separately for HV1 and for HV2, resulting in the learned delays $\tau_1 = 1.16\,\mathrm{s}$ and $\tau_2 = 0.92\,\mathrm{s}$, respectively. These are in the realistic domain corresponding to other measurements in the literature [31]–[33]. The final learned equation of motion of the three vehicles on the virtual ring is given by the neural delay differential equation (NDDE):

$$\dot{h}_1(t) = v_2(t) - v_1(t)\,, \tag{21}$$

$$\dot{h}_2(t) = v_3(t) - v_2(t)\,, \tag{22}$$

$$\dot{v}_1(t) = \mathrm{net}_1(h_1(t-\tau_1), v_1(t-\tau_1), \Delta v_{21}(t-\tau_1))\,, \tag{23}$$

$$\dot{v}_2(t) = \mathrm{net}_2(h_2(t-\tau_2), v_2(t-\tau_2), \Delta v_{32}(t-\tau_2))\,, \tag{24}$$

$$\begin{aligned}\dot{v}_3(t) = \mathrm{sat}\Big(&\alpha\big(V(h_3(t-\sigma)) - v_3(t-\sigma)\big)\\ &+ \beta\big(W(v_1(t-\sigma)) - v_3(t-\sigma)\big)\Big)\,,\end{aligned} \tag{25}$$

where net_1 and net_2 are the human driver dynamics captured by the TDNNs.

Figure 3 presents the acceleration of the vehicles in the plane of the headway h and the relative velocity Δv, while the velocity is fixed at $20\,\mathrm{m/s}$. Since the controls of the AV and the accelerations of the HVs depend on three inputs, their visualization is possible only by fixing one variable. Note

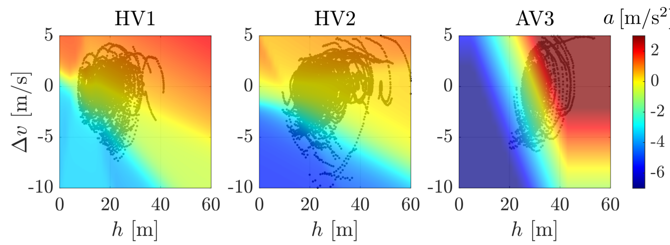

Fig. 3. Acceleration of the three vehicles as a function of the headway and relative velocity, while the vehicle's own speed is fixed to $v = 20\,\mathrm{m/s}$. In the case of HV1 and HV2, the coloring reflects the learned dynamics, while in the case of AV3 the control was known (here $h_{\mathrm{go}} = 42.5\,\mathrm{m}$). The dots indicate those states during the experiments where the vehicle's own velocity was between $17\,\mathrm{m/s}$ and $23\,\mathrm{m/s}$.

that the control parameters of the AV are set according to Table I, while its free-flow headway is $h_{\mathrm{go}} = 42.5\,\mathrm{m}$. In each panel, gray dots refer to those $(h, \Delta v)$ combinations, which occurred during the experiment such that the velocity was approximately $20\,\mathrm{m/s}$ (more precisely $17\,\mathrm{m/s} < v < 23\,\mathrm{m/s}$). Thus, in the case of the HVs, the region covered by gray dots is where the TDNN interpolates, while the complement domain is obtained with extrapolation only.

All panels in Fig. 3 depict large decelerations (brakings) when the headway is small, while the relative velocity is negative. Both the increase of h and that of Δv yield increasing accelerations. This matches our expectations. The results also show that the driver of HV2 is more cautious than the driver of HV1. In case of HV1 and AV3, the zero acceleration (yellow) combinations can be approximated well with a stripe of negative slope, while in case of HV2, almost zero acceleration occurs over a larger domain, also indicating the cautiousness of the driver. Of the three vehicles, the AV is the most sensitive to changes in the relative velocity, while it keeps the largest headway.

The learned dynamical system can perform bistable behavior when the learned reaction times of the human drivers are slightly increased, which also occurs in real driving scenarios. For simplicity, in the following analysis, we assume that the reaction times of the drivers are the same $\tau_1 = \tau_2 = \tau$ while the weights and biases in each human driver model are individually learned and carried over. The corresponding bistable behavior is shown in Fig. 4, which presents the time profiles of the velocities and headways obtained by simulating the NDDE (21)-(25). The free-flow headway of the AV is $h_{\mathrm{go}} = 42.5\,\mathrm{m}$, the human time delay $\tau = 1.5\,\mathrm{s}$ and the net length of the virtual ring is $L = 75\,\mathrm{m}$. The initial conditions are selected as $v_1(t) = v_2(t) = v_3(t) = 15\,\mathrm{m/s}$, $h_1(t) = h_2(t) = 20\,\mathrm{m}$, for $t \in [-\tau, 0]$; this results in $h_3(t) = 35\,\mathrm{m}$ according to (7).

After a few oscillations, the system converges to a stable steady state motion where all vehicles travel at approximately $23\,\mathrm{m/s}$, while their headways settle at different distances determined by the individual controllers. Then, at $t = 100\,\mathrm{s}$, HV1 performs a constant-deceleration braking for 1.5 seconds, similar to the intentional braking of the last driver in the field experiment, see Fig. 2. After this braking, the velocity of HV1

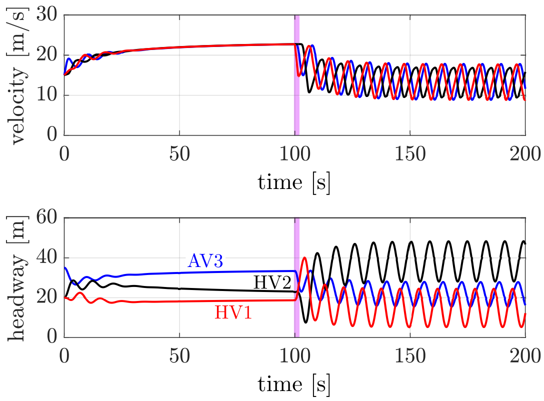

Fig. 4. Time profiles obtained by simulating the learned human driver dynamics for $L = 75\,\mathrm{m}$, $h_{\mathrm{go}} = 42.5\,\mathrm{m}$, $\tau_1 = \tau_2 = 1.5\,\mathrm{s}$. The red, black and blue colors refer to vehicles HV1, HV2 and AV3, respectively. Similarly to the experiments, the initial transients are decaying and the system tends to a stable steady state solution, however, when HV1 brakes intentionally, the perturbation is large enough to "kick" the system out of the basin of attraction of the equilibrium, and oscillations converge to a stable limit cycle. This shows the bistable nature of the learned nonlinear system.

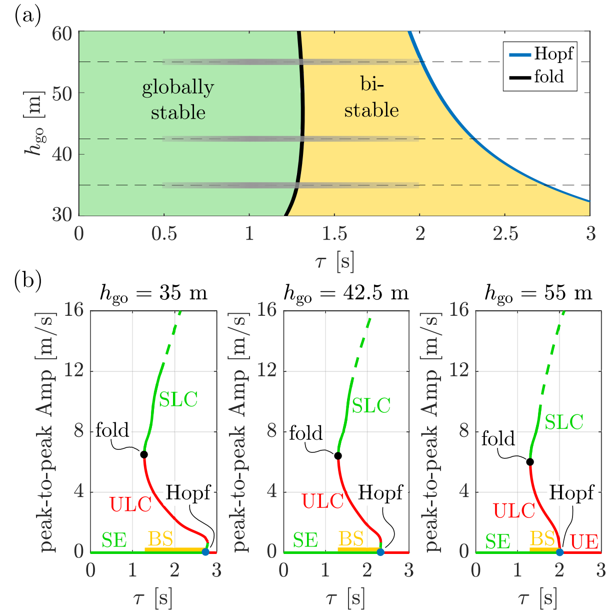

Fig. 5. (a) Stability chart of the system in the plane of the time delay of the human drivers (assumed to be the same for HV1 and HV2) and the free-flow headway of the AV for net ring length $L = 75\,\mathrm{m}$. The blue curve indicates Hopf bifurcation, while the black curve shows the location of the fold of the limit cycles. The latter one divides the stable area into a globally stable (green) and into a bistable (orange) domain. The gray zones indicate those domains where the neural networks could interpolate. (b) Bifurcation diagrams for various values of the free-flow headway h_{go} of the AV. Stable and unstable solutions are indicated using red and green colors. The bistable domains are also indicated as orange.

is almost the same as its initial velocity. The resulting vibrations do not decay, but in contrast, they converge to a stable oscillatory motion, called a limit cycle. The mean velocity of this limit cycle is smaller than the previous equilibrium velocity, and the headways change as well: the headway of HV2 increases, while that of AV3 decreases. Although, this shift in the mean value of the velocities and headways was not always present in the measurements, the obtained bistable behavior is qualitatively the same as that observed in the experiments.

To better understand under what parameters the system can be bistable, we carry out bifurcation analysis with the help of the MATLAB package DDE-BIFTOOL [34]. This allows us to find stable and unstable motions and continue these as the system parameters are varied.

Figure 5(a) presents the stability chart of the system in the plane of the human time delay τ and the free-flow headway h_{go} of the AV. The blue curve indicates the Hopf bifurcation boundary, on the left-hand side of which the steady state (also called equilibrium) is stable. In the green domain, the equilibrium is globally stable, that is, the oscillations die out after any large perturbation and the state of the system returns to its equilibrium. In contrary, in the orange domain the system is bistable meaning that the trajectories may converge to the (locally) stable equilibrium or to the (locally) stable limit cycle depending on the perturbations.

The Hopf bifurcation boundary shows that the decrease of h_{go} allows the HVs to operate with larger delays, which can be explained by the fact that the smaller the value of h_{go} is, the smaller h_3 will be and thus the larger the headway of human drivers can be. In those large delay domains, the system is strongly bistable. The horizontal dashed lines correspond to those values of h_{go} where the experiments were carried out and the gray stripes indicate the plausible time delays of human drivers shaded according to the probability of the given time delay. Note that the human reaction time is not described with a symmetric distribution, rather with a gamma distribution, which is elongated more to the right, that is, to larger time delay values [33], [35].

Figure 5(b) presents bifurcation diagrams for fixed values of h_{go}. The time delay τ of the human drivers is selected as the bifurcation parameter, while the vertical axis is the peak-to-peak amplitude of the velocity of HV1. The stable equilibrium (SE) and the stable limit cycle (SLC) are denoted by green curves, while the red curves represent the unstable equilibrium (UE) and the unstable limit cycle (ULC). The bistable domain (BS) is indicated as orange. Initially, a branch of SLC emerges from the Hopf point, but almost immediately it turns left and becomes ULC. Then, there is a fold in this branch at around $\tau \approx 1.3$ s, above which the limit cycle becomes stable. As the amplitude increases, there is a point at which at least one of the headways becomes negative, that is, the cars collide. This is indicated by the dashed green curves and highlights the potential detrimental effect of increased driver reaction time delays.

V. Conclusion

In this paper, we presented experimental results with an AV and two HVs, and learned the human driving dynamics based on the collected experimental data. The virtual ring concept allowed the vehicles to travel on a straight road with realistic speeds. The measurements were carried out with various control setups of the AV, some of which led to bistable behavior.

Based on the measurement data, we learned the human driving dynamics for the two human drivers using time delay neural networks. The networks were substituted into the mathematical model of the virtual ring configuration, and the simulation of the resulting neural delay differential equations showed similar bistable behavior as observed in the experiments. Besides, we also presented a stability chart and bifurcation diagrams to visualize the critical parameter combinations at which the equilibrium is not globally stable.

The results support a better understanding of human driver behavior, which is key when designing the control algorithms for self-driving cars, so that they can operate safely and efficiently in mixed traffic situations.

In the future, we plan to analyze the effect of different human reaction times, which may lead to even more intricate dynamical phenomena. Furthermore, the model of the neural network could be further generalized, for example, using different delays for the inputs. However, when using such models, special care must be taken not to overfit the data.

ACKNOWLEDGMENT

The authors acknowledge the help of Chaozhe He in collecting the experimental data.

REFERENCES

[1] S. E. Shladover, D. Su, and X.-Y. Lu, "Impacts of cooperative adaptive cruise control on freeway traffic flow," *Transportation Research Record*, vol. 2324, no. 1, pp. 63–70, 2012.

[2] S. Öncü, J. Ploeg, N. van de Wouw, and H. Nijmeijer, "Cooperative adaptive cruise control: network-aware analysis of string stability," *IEEE Transaction on Intelligent Transportation Systems*, vol. 15, no. 4, pp. 1527–1537, 2014.

[3] G. Orosz, "Connected cruise control: modelling, delay effects, and nonlinear behaviour," *Vehicle System Dynamics*, vol. 54, no. 8, pp. 1147–1176, 2016.

[4] Y. Qin, H. Wang, and B. Ran, "Control design for stable connected cruise control systems to enhance safety and traffic efficiency," *IET Intelligent Transport Systems*, vol. 12, no. 8, pp. 921–930, 2018.

[5] G. Orosz and T. G. Molnár, *Dynamics and Control of Connected Vehicles*. Springer, 2025.

[6] T. G. Molnár, M. Hopka, D. Upadhyay, M. Van Nieuwstadt, and G. Orosz, "Virtual rings on highways: Traffic control by connected automated vehicles," in *AI-enabled Technologies for Autonomous and Connected Vehicles*. Springer, 2023, pp. 441–479.

[7] B. Szaksz, G. Orosz, and G. Stepan, "Guided control of a human driver via an automated vehicle," *IFAC-PapersOnLine*, vol. 56, no. 2, pp. 899–904, 2023.

[8] J. Wang, Y. Zheng, C. Chen, Q. Xu, and K. Li, "Leading cruise control in mixed traffic flow: System modeling, controllability, and string stability," *IEEE Transactions on Intelligent Transportation Systems*, vol. 23, no. 8, pp. 12 861–12 876, 2021.

[9] Y. Sugiyama, M. Fukui, M. Kikuchi, K. Hasebe, A. Nakayama, K. Nishinari, S. Tadaki, and S. Yukawa, "Traffic jams without bottlenecks – experimental evidence for the physical mechanism of the formation of a jam," *New Journal of Physics*, vol. 10, no. 3, p. 033001, 2008.

[10] R. E. Stern, S. Cui, M. L. Delle Monache, R. Bhadani, M. Bunting, M. Churchill, N. Hamilton, R. Haulcy, H. Pohlmann, F. Wu, B. Piccoli, B. Seibold, J. Sprinkle, and D. B. Work, "Dissipation of stop-and-go waves via control of autonomous vehicles: Field experiments," *Transportation Research Part C*, vol. 89, pp. 205–221, 2018.

[11] M. Pooladsanj, K. Savla, and P. A. Ioannou, "Vehicle following on a ring road under safety constraints: Role of connectivity and coordination," *IEEE Transactions on Intelligent Vehicles*, vol. 8, no. 1, pp. 628–638, 2022.

[12] S. S. Avedisov, G. Bansal, and G. Orosz, "Impacts of connected automated vehicles on freeway traffic patterns at different penetration levels," *IEEE Transactions on Intelligent Transportation Systems*, vol. 23, no. 5, pp. 4305–4318, 2022.

[13] B. Szaksz, T. G. Molnar, S. S. Avedisov, G. Stepan, and G. Orosz, "Connected vehicle experiments on virtual rings: Unveiling bistable behavior," in *IEEE Intelligent Vehicles Symposium*. IEEE, 2025, pp. 1014–1019.

[14] X. A. Ji, T. G. Molnár, A. A. Gorodetsky, and G. Orosz, "Bayesian inference for time delay systems with application to connected automated vehicles," in *24th IEEE International Conference on Intelligent Transportation Systems*. IEEE, 2021, pp. 3259–3264.

[15] S. Theodoridis, *Machine learning: a Bayesian and optimization perspective*. Academic Press, 2015.

[16] M. Cenedese, J. Axås, B. Bäuerlein, K. Avila, and G. Haller, "Data-driven modeling and prediction of non-linearizable dynamics via spectral submanifolds," *Nature Communications*, vol. 13, no. 1, p. 872, 2022.

[17] J. Axås, M. Cenedese, and G. Haller, "Fast data-driven model reduction for nonlinear dynamical systems," *Nonlinear Dynamics*, vol. 111, no. 9, pp. 7941–7957, 2023.

[18] S. L. Brunton, J. L. Proctor, and J. N. Kutz, "Discovering governing equations from data by sparse identification of nonlinear dynamical systems," *Proceedings of the National Academy of Sciences*, vol. 113, no. 15, pp. 3932–3937, 2016.

[19] Á. T. Köpeczi-Bócz, H. Sykora, and D. Takács, "Data-driven delay identification with SINDy," in *Advances in Nonlinear Dynamics*, W. Lacarbonara, Ed., vol. III. Springer, 2024, pp. 481–491.

[20] Q. Li, F. Dietrich, E. M. Bollt, and I. G. Kevrekidis, "Extended dynamic mode decomposition with dictionary learning: A data-driven adaptive spectral decomposition of the koopman operator," *Chaos: An Interdisciplinary Journal of Nonlinear Science*, vol. 27, no. 10, 2017.

[21] X. A. Ji and G. Orosz, "Trainable delays in time delay neural networks for learning delayed dynamics," *IEEE Transactions on Neural Networks and Learning Systems*, vol. 36, no. 3, pp. 5219–5229, 2025.

[22] M. Zhou, X. Qu, and X. Li, "A recurrent neural network based microscopic car following model to predict traffic oscillation," *Transportation Research Part C*, vol. 84, pp. 245–264, 2017.

[23] G. Stépán, *Retarded Dynamical Systems*. Longman, 1989.

[24] X. A. Ji and G. Orosz, "Learning time delay systems with neural ordinary differential equations," *IFAC-PapersOnLine*, vol. 55, no. 36, pp. 79–84, 2022.

[25] X. Zhang, X. Xu, and Y. Zhu, "An improved time delay neural network model for predicting dynamic heat and mass transfer characteristics of a packed liquid desiccant dehumidifier," *International Journal of Thermal Sciences*, vol. 177, p. 107548, 2022.

[26] C. Marcus and R. Westervelt, "Stability of analog neural networks with delay," *Physical Review A*, vol. 39, no. 1, p. 347, 1989.

[27] M. Bando, K. Hasebe, A. Nakayama, A. Shibata, and Y. Sugiyama, "Dynamical model of traffic congestion and numerical simulation," *Physical Review E*, vol. 51, no. 2, pp. 1035–1042, 1995.

[28] M. Bando, K. Hasebe, K. Nakanishi, and A. Nakayama, "Analysis of optimal velocity model with explicit delay," *Physical Review E*, vol. 58, no. 5, pp. 5429–5435, 1998.

[29] X. Glorot and Y. Bengio, "Understanding the difficulty of training deep feedforward neural networks," in *13th International Conference on Artificial Intelligence and Statistics*, vol. 9. PMLR, 2010, pp. 249–256.

[30] D. P. Kingma, "Adam: A method for stochastic optimization," *3rd International Conference on Learning Representations*, 2015.

[31] A. Mehmood and S. M. Easa, "Modeling reaction time in car-following behaviour based on human factors," *International Journal of Applied Science, Engineering and Technology*, vol. 5, no. 2, pp. 93–101, 2009.

[32] J. I. Ge and G. Orosz, "Connected cruise control among human-driven vehicles: Experiment-based parameter estimation and optimal control design," *Transportation Research Part C*, vol. 95, pp. 445–459, 2018.

[33] B. Szaksz, G. Orosz, and G. Stepan, "Guided control of human drivers: Control design and experiments," *IEEE Transactions on Control Systems Technology*, vol. 33, no. 6, pp. 2455–2462, 2025.

[34] K. Engelborghs, T. Luzyanina, and D. Roose, "Numerical bifurcation analysis of delay differential equations using DDE-BIFTOOL," *ACM Transactions on Mathematical Software*, vol. 28, no. 1, pp. 1–21, 2002.

[35] R. Ratcliff, "Group reaction time distributions and an analysis of distribution statistics." *Psychological Bulletin*, vol. 86, no. 3, p. 446, 1979.